Iron L-Edge X-ray Absorption Spectroscopy of Myoglobin Complexes and Photolysis Products

Hongxin Wang,[†] Gang Peng,[‡] Lisa M. Miller,[†,§] Eva M. Scheuring,[§] S. J. George,[‡] Mark R. Chance,*[,§] and Stephen P. Cramer*[,†,‡]

Contribution from the Energy and Environment Division, Lawrence Berkeley National Laboratory, Berkeley, California 94720, Department of Applied Science, University of California, Davis, California 95616, and Department of Physiology and Biophysics, Albert Einstein College of Medicine of Yeshiva University, Bronx, New York 10461

Received May 1, 1996[⊗]

Abstract: We demonstrate the first application of L-edge X-ray absorption spectroscopy (XAS) to the electronic characterization of biological photolysis products. The experimental L-edge XAS spectra of deoxymyoglobin (deoxy Mb), oxymyoglobin (MbO_2), carbonmonoxymyoglobin (MbCO), and the low-temperature photoproducts (Mb*CO and Mb*O_2) are presented and compared to simulated spectra using a ligand field multiplet calculation. This analysis indicates that MbCO and MbO_2 are both low spin and does not support some previous studies which suggest that MbO_2 has an intermediate spin. Both photoproducts, Mb*CO and Mb*O_2, are different from deoxy Mb in the Fe^{II} electronic structure. In addition, different low-temperature photolysis intermediates are suggested for MbCO and MbO_2. The L-edge XAS spectra for Fe^{III} in aquometmyoglobin (met Mb) and azidomet myoglobin (MbN_3) provide a comparison of the ferrous versus ferric myoglobin species. Finally, the special advantages of using soft X-ray absorption spectroscopy for understanding the electronic transitions coupled to photolysis-induced structural changes are discussed.

Introduction

The process of photodissociation in which bonds are broken following absorption of a photon is of fundamental importance in biology and chemistry.[1−3] Photochemically generated intermediates can initiate subsequent reactions and produce special products for various scientific and industrial applications.[1] X-ray absorption spectroscopy (XAS) has been used to characterize a number of photochemically generated samples which contain metal centers, especially in the area of biophysics. In one of the first solution studies, Mills et al.[4−7] used a 20-Hz repetition rate Nd:YAG laser to photolyze carbonmonoxymyoglobin (MbCO), and they monitored the photolysis product (Mb*CO) with time-resolved K-edge XAS. Since then, other systems for time-resolved K-edge XANES and EXAFS have been used by Clozza et al.,[8] by Thiel et al.,[9] and by Chance et al.[10] on flowing solution samples. K-edge XAS without rapid time resolution has also been used to study various trapped intermediate photoproducts such as low-temperature myoglobin and hemoglobin photoproducts,[11−13] and the S states in photosystem II.[14] Meanwhile, time-resolved K-edge XAS has been used in various fields to characterize the changes in gas-phase plasmas,[15] ablated particles,[16] doped glasses,[17] and solid state material samples[18] following laser irradiation. To date, all XAS applications on biological photoproducts have only involved the use of hard X-ray radiation (>2000 eV).

L-edge XAS of the first row (3d) transition metals, which utilizes soft X-rays in the energy region of 500−1000 eV, has several advantages over K-edge XAS.[19] Generally, soft X-ray XAS has 3−5 times better energy resolution, resulting in sharper spectral features. Transitions at the L edge ($2p \rightarrow 3d$) are dipole-allowed and provide spectra that are more intense and structured than the dipole-forbidden K-edge ($1s \rightarrow 3d$) transitions. This is especially valuable for studying ligand association and dissociation in metalloproteins, such as hemeproteins, where the metal (3d) orbitals are the ligand-bonding orbitals. In addition, L-edge XAS spectra can be interpreted by ligand field calculations,[20−23] which provide a more detailed understanding of metalloprotein electronic structures. L-edge XAS is sensitive

* Address correspondence to these authors.
† Lawrence Berkeley National Laboratory.
‡ University of California.
§ Albert Einstein College of Medicine of Yeshiva University.
⊗ Abstract published in *Advance ACS Abstracts,* March 1, 1997.

(1) Bershon, R. In *Molecular Photodissociation Dynamics*; Ashford, M. N. R., Baggot, J. E., Eds.; Royal Society of Chemistry: London, 1987; p 61.
(2) Wang, H.; Chen, X.; Weiner, B. R. *J. Phys. Chem.* **1993**, *97*, 12261.
(3) Chen, X.; Wang, H.; Weiner, B. R.; Hawley, M.; Nelson, H. H. *J. Phys. Chem.* **1993**, *97*, 12269.
(4) Mills, D. M. *Phys. Today* **1984**, *4*, 22.
(5) Mills, D. M.; Pollock, V.; Lewis, A.; Harootian, A.; Huang, J. *Nucl. Instrum.* **1984**, *222*, 351.
(6) Mills, D. M.; Lewis, A.; Harootian, A.; Huang, J.; Smith, B. *Science* **1984**, *223*, 811.
(7) Pollock, V.; Mills, D. M. *Nucl. Instrum. Methods* **1984**, *A226*, 668.
(8) Clozza, A.; Castellano, A. C.; Longa, S. D.; Giovannelli, A.; Bianconi, A. *Rev. Sci. Instrum.* **1989**, *60*, 2519.
(9) Thiel, D. J.; Livins, P.; Stern, E. A.; Lewis, A. *Nature* **1993**, *362*, 40.
(10) Chance, M. R.; Wirt, M. D.; Scheuring, E. M.; Miller, L. M.; Xie, A.; Sidelinger, D. *Rev. Sci. Instrum.* **1993**, *64*, 2035.
(11) Chance, B.; Fischetti, R.; Powers, L. *Biochemistry* **1983**, *22*, 3820.
(12) Powers, L.; Chance, B.; Chance, M. R.; Campbell, B.; Friedman, J.; Khalid, S.; Kumar, C.; Naqui, A.; Reddy, K. S.; Zhou, Y. *Biochemistry* **1987**, *26*, 4785.
(13) Chance, M. R.; Miller, L. M.; Fischetti, R. F.; Scheuring, E.; Huang, W. X. Sclavi, B.; Hai, Y.; Sullivan, M. *Biochemistry* **1996**, *35*, 9014.
(14) Yachandra, V. K.; Guiles, R. D.; McDermott, A. E.; Cole, J. L.; Zimmermann, V. L. J.; Sauer, K.; Klein, M. K. *Phys. B* **1989**, *158*, 78.
(15) Wang, L. S.; Lin, Z. Q.; Zhang, H. H.; He, X. F. *Acta Phys. Sin. (Overseas Ed.)* **1994**, *3*, 909.
(16) Ohyanagi, T.; Miyashita, A.; Murakami, K. *J. Appl. Phys., Part I* **1994**, *33*, 2586.
(17) Lee, J. M.; Paesler, M. A.; Sayers, D. E.; Fontaine, A. *Phys. B* **1989**, *158*, 52.
(18) Kassner, M. E.; Li, X.; McQueen, H. J. *Mater. Sci. Eng.* **1993**, *A169*, 9.
(19) Cramer, S. P.; deGroot, F. M. K.; Ma, Y.; Chen, C. T.; Sette, F.; Kipke, C. A.; Eichhorn, D. M.; Chan, M. K.; Armstrong, W. H.; Libby, E.; Christou, G.; Brooker, S.; McKee, V.; Mullins, O. C.; Fuggle, J. C. *J. Am. Chem. Soc.* **1991**, *113*, 7937.

S0002-7863(96)01446-1 CCC: $14.00

to oxidation states and spin states, and has been used to characterize metal centers in various manganese,[19] iron,[24] nickel,[25] and copper[26] model compounds and proteins. Until now, however, no work on L-edge XAS characterization of biochemical photoreaction intermediates has been reported.

Myoglobin is one of the most well-characterized metalloproteins. Its function is to facilitate the diffusion of oxygen in muscle cells. In addition to binding O_2, the ferrous iron in myoglobin also binds other diatomic ligands such as CO and NO. Understanding the mechanism by which myoglobin discriminates between ligands (*e.g.* in favor of O_2) has been the subject of many studies over the past 40 years. The iron−ligand bond can be broken with a single photon of light.[4] Thus, photoreactions coupled with spectroscopic techniques including visible,[27,28] infrared,[27−29] resonance Raman,[30−34] nuclear magnetic resonance (NMR),[35] electron paramagnetic resonance (EPR),[36−38] Mössbauer,[39,40] X-ray absorption,[4−8,10] and X-ray crystallography[41−43] have been used to examine the ligand-binding and ligand-dissociation natures of these hemeproteins. The results have clearly demonstrated differences between the ligand-binding pathways of O_2, CO, and NO.

Upon photolysis of a ligand, the heme iron undergoes both structural and electronic changes.[4] The recent low-temperature (20 K) crystallography on the MbCO photoproduct (Mb*CO) has demonstrated the geometry of the photodissociated intermediate state.[43] Although some theoretical and experimental results[29,44,45] have alluded to the electronic structure of Mb*CO, L-edge XAS provides the first direct probe of the Mb*CO (iron 3d) orbital configuration. In contrast to Mb*CO, little is known about the structure of the MbO_2 photoproduct (Mb*O_2). L-edge measurements can reveal the detailed electronic information necessary to interpret electronic difference between Mb*CO and Mb*O_2, while complementing the structural information obtained through K-edge EXAFS and X-ray crystallography.

This paper demonstrates the first application of L-edge XAS in conjunction with a biological photoreaction, and illustrates the power of the method for understanding electronic transitions coupled to photolysis-induced structural changes. The L-edge XAS spectra for the ligand-bound species, MbCO and MbO_2, are compared with their corresponding photolysis products, Mb*CO and Mb*O_2, and to the unligated state, deoxy Mb. These spectra have also been simulated using a ligand field multiplet calculation so that similarities and differences in the 3d orbital configurations for these species can be elucidated. The analytical results, compared with the available structural information about the myoglobin species, provide an excellent test system for this technique. Finally, special advantages of using L-edge XAS for characterizing photolysis intermediates are discussed.

Experimental Section

Sample Preparation. Horse skeletal muscle myoglobin (Sigma, 99.5%) was dissolved into 100 mM potassium phosphate buffer, pH 7, and stirred on ice for 10 min. This aquometmyoglobin (met Mb) sample was centrifuged at 10 °C for 20 min and then transferred to a nitrogen-atmosphere glovebox. Azidometmyoglobin (MbN_3) was prepared from met Mb by the addition of a 10-fold excess of sodium azide (Na_3N_3, Sigma, 99.9%). For the ferrous samples, after stirring under nitrogen for 15 min, sodium dithionite ($Na_2S_2O_4$, Aldrich, 99.9%) was added to the solution in a 5-fold excess to obtain deoxy Mb. MbCO (and MbO_2) were prepared by continuously blowing CO (or O_2) gas (MG Industries) over a deoxy Mb sample for 5 min. A UV−visible spectrum indicated that the samples were greater than 95% deoxy Mb, MbCO, or MbO_2.[46] Solution samples were then spread onto gold-plated copper sample holders and partially dehydrated in a desiccator under a nitrogen environment at 4 °C. The partially dehydrated thin films (0.5 mm thick) had an estimated concentration of 20−30 mM. After data collection, sample integrity was confirmed by examining the UV−visible spectra of the redissolved (into degassed buffer) Mb films.

XAS Measurement. The apparatus for collecting L-edge X-ray absorption spectra is schematically shown in Figure 1. The experiments were performed at the Stanford Synchrotron Radiation Laboratory (SSRL), beamline 10-1. The X-ray beam was adjusted to a spot size of 2×2 mm^2 with an energy resolution of 0.4 eV. Windowless operation was used from the storage ring to the 13-element germanium detector,[47] with a chamber vacuum of 3×10^{-9} Torr. The detector was positioned at 90° with respect to the incoming X-ray beam and the sample orientation was adjusted to maximize the X-ray fluorescence signal. A 2 μm thick parylene filter was placed between the sample and the detector to preferentially filter out oxygen K_α fluorescence. The partially dehydrated samples were inserted through a load-lock and mounted onto the precooled (10 K) cold finger. For data collection, the iron fluorescence signal (F) was normalized to the incident X-ray flux (I_0), measured by electron yield from a gold-coated grid. Scans were collected in 0.15-eV steps at 3 s/point integration time. Each spectrum is a sum of 20 scans. L-edge positions were calibrated using Fe_2O_3 as a reference, where the L_3 peak falls at 709.1 eV. The photolysis of myoglobin (MbCO and MbO_2) was done by illuminating the sample with a continuous wave (cw) He−Ne laser (MWK, 633 nm, 10 mW) for 30 min.

XAS Analysis. For comparison with the theoretical simulation, the residual background of each spectrum was first removed by fitting a 4th order polynomial function to the data in front of the L_3 and beyond the L_2 edge. The peak positions of L_3 and L_2 are defined as the points

(20) de Groot, F. M. F.; Fuggle, J. C.; Thole, B. T.; Sawatzky, A. *Phys. Rev.* **1990**, *42*, 5459.
(21) de Groot, F. M. F. *J. Electron Spectrosc. Relat. Phenom.* **1994**, *67*, 529.
(22) de Groot, F. M. F.; Arrio, M. A.; Sainctavit, P.; Cartier, C.; Chen, C. T. *Solid State Commun.* **1994**, *92*, 991.
(23) van der Laan, G.; Kirkman, I. W. J. *Phys. Condens. Matters* **1992**, *4*, 4189.
(24) Peng, G.; van Elp, J.; Jang, H.; Que, L.; Armstrong, W. H.; Cramer, S. P. *J. Am. Chem. Soc.* **1995**, *117*, 2515.
(25) van Elp, J.; Peng, G.; Zhou, Z. H.; Adams, M. W. W.; Baidya, N.; Mascharak, P. K.; Cramer, S. P. *Inorg. Chem.* **1995**, *34*, 2503.
(26) George, S. J.; Lomery, M. D.; Solomon, E. I.; Cramer, S. P. *J. Am. Chem. Soc.* **1993**, *115*, 2968.
(27) Steinbach, J. P. *Biochemistry* **1991**, *30*, 3988.
(28) Miller, L. M.; Chance, M. R. *Biochemistry* **1995**, *34*, 10170.
(29) Miller, L. M.; Chance, M. R. *J. Am. Chem. Soc.* **1994**, *116*, 9662.
(30) Spiro, T. G.; Burke, J. M. *J. Am. Chem. Soc.* **1976**, *98*, 5482.
(31) Rousseau, D. L.; Argade, P. *Proc. Natl. Acad. Sci. U.S.A.* **1986**, *83*, 1310.
(32) Hoard, J. L. *Science* **1971**, *174*, 1295.
(33) Rousseau, D. L.; Friedman, J. M. In *Biological Applications of Raman Spectroscopy*; John Wiley and Sons: New York, 1988; p 135.
(34) Spiro, T. G.; Stong, J. D.; Stein, P. *J. Am. Chem. Soc.* **1979**, *101*, 2648.
(35) Keating, K. A.; LaMar, G. N.; Shiav, F. Y.; Smith, K. M. *J. Am. Chem. Soc.* **1992**, *114*, 6513.
(36) Hoffman, B. M.; Petering, D. H. *Proc. Natl. Acad. Sci. U.S.A.* **1970**, *67*, 637.
(37) Chien, J. C. W.; Dickinson, L. C. *Proc. Natl. Acad. Sci. U.S.A.* **1972**, *69*, 2783.
(38) Yonetani, T.; Yamamato, H.; Iizuka, T. *J. Biol. Chem.* **1974**, *249*, 2168.
(39) Spartalian, K.; Lang, G.; Yonetani, T. *Biochim. Biophys. Acta* **1976**, *428*, 281.
(40) Marcolin, H. E.; Reschke, R.; Trautwein, A. *Eur. J. Biochem.* **1979**, *96*, 119.
(41) Phillips, S. E. V. *Brookhaven Protein Data Bank* **1981**,
(42) Quillin, M. L.; Arduini, R. M.; Olson, J. S.; Phillips, G. N. *J. Mol. Biol.* **1993**, *234*, 140.
(43) Schlichting, I.; Berendsen, J.; Phillips, G. N.; Sweet, R. M. *Nature* **1994**, *371*, 808.
(44) Chance, M. R.; Courtney, S. H.; Chavez, M. D.; Ondrias, M. R.; Friedman, J. M. *Biochemistry* **1990**, *29*, 5537.
(45) Petrich, J.; Poyart, C.; Martin, J. *Biochemistry* **1988**, *27*, 4049.
(46) Antonini, E.; Brunori, M. *Hemoglobin and Myoglobin in Their Reactions with Ligands*; North-Holland: New York, 1971.
(47) Cramer, S. P.; Chen, J.; George, S. J.; van Elp, J.; Moore, J.; Teusch, O.; Colaresi, J.; Yocum, M.; Mullins, O. C.; Chen, C. T. *Nucl. Instrum. Methods Phys. Res.* **1992**, *A319*, 285.

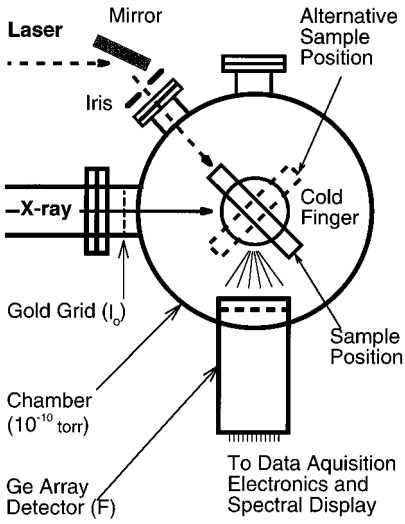

Figure 1. Experimental setup for collecting L-edge X-ray absorption spectra on the ligand-bound and photoproduct states of myoglobin. Windowless operation was used between the X-ray storage ring, sample, and 13-element germanium detector, where all were maintained under high-vacuum (3×10^{-9} Torr) conditions. The iron fluorescence signal (F) was normalized to the incident X-ray flux (I_0), as measured from a gold grid. For photolysis, the cold finger was rotated 90° and the sample was photolyzed with a continuous-wave He−Ne laser (633 nm, 10 mW) for 30 min.

Table 1. X-ray Edge Positions (L_3 and L_2) and Branching Ratios (Observed and Corrected) for Various Myoglobin Species

	peak positions, eV L_3 (L_2)	branching ratios	
		obsd (errors)	corrected (errors)
deoxy Mb	708.00	0.68	0.76
	(718.50)	(±0.01)	(±0.01)
MbCO	708.15	0.59	0.67
	(718.80)	(±0.01)	(±0.01)
Mb*CO	708.00	0.70	0.77
	(718.65)	(±0.01)	(±0.01)
MbO_2	708.00	0.60	0.68
	(718.80)	(±0.01)	(±0.01)
Mb* + O_2	707.85	0.65	0.72
	(718.50)	(±0.02)	(±0.02)
met Mb	709.30	0.68	0.76
	(720.30)	(±0.01)	(±0.01)
MbN_3	709.40	0.59	0.67
	(720.40)	(±0.01)	(±0.01)

with maximum intensities in the measured XAS spectrum. Experimental branching ratios (R_{obs}) are defined as follows: $R_{obs} = L_3/(L_2 + L_3)$, where L_i ($i = 2, 3$) is the integrated intensity for the observed L_i peak. The uncertainties (ΔL_2 and ΔL_3) for the L_3 and L_2 integrals are calculated from the signal-to-noise ratio of each spectrum in the regions of the L_3 and L_2 edges. For all of the myoglobin spectra in this study, $\Delta L_2/L_2 \cong \Delta L_3/L_3 \cong \Delta L/L \cong 0.004$. The uncertainty in the branching ratio, ΔR, was estimated as $\Delta R/R \cong 2(\Delta L/L)$. This leads to an estimated value for $\Delta R/R \cong 0.008$ and a value for ΔR of less than 0.01 for all the myoglobin species except Mb* + O_2. Since the Mb* + O_2 spectrum is a difference of two experimental spectra and its intensity is about 50% of the experimental Mb*O_2 spectrum, the error in the difference spectrum, $\Delta L'/L'$, becomes $\{2(\Delta L/L)^2\}^{1/2}/0.50$. Therefore, ΔR for Mb* + O_2 is estimated to be about 0.02. All of the branching ratios and their errors are listed in Table 1.

The calculations for the simulated XAS spectra were performed by published methods.[19−26] For Fe^{II}, the calculation describes the electronic transitions from $3d^6$ ground state to $2p3d^7$, where $2p$ stands for the 2p core hole. For Fe^{III}, the calculation simulates the electronic transitions from $3d^5$ ground state to $2p3d^6$. Coulomb and exchange interactions and spin−orbital interactions for both initial (2p) and final (3d) states were first calculated. Atomic multiplets were used to account for the ground and final state electronic spin−orbital L−S interactions and the final state 2p core hole $J-J$ coupling. The *ab initio* Hartree−Fock values of Slater integrals and spin−orbital couplings (2p and 3d) for the 3d transition metals were used as tabulated values. Charge transfer and electron correlation effects were accounted for by reducing the *ab initio* Hartree−Fock values of the Coulomb and exchange integrals to 70% of the calculated values. The calculated atomic multiplets were projected to the eigenstates for the iron in ligand field.

To describe the local symmetry, ligand field parameters were added. The local symmetry of the iron sites in all myoglobin species (either five-coordinate pyramidal or six-coordinate ML_4XY) is similar to a D_{4h} symmetry[48−50] and can be started with a regular O_h symmetry.[51] In O_h symmetry, the 3d orbitals are split into t_{2g} and e_g classes with an energy difference of $10D_q$. In lowering the symmetry from O_h to a distorted D_{4h}, two more parameters (D_s and D_t) are introduced. The calculated spectra were broadened with a Lorentzian and a Gaussian, to describe the lifetime and instrumental broadening, respectively. The ligand field parameters ($10D_q$, D_s and D_t) were adjusted to obtain the best fit to the experimental XAS spectra. Iron (3d) energy diagrams were constructed with these parameters, using a standard formula.[51]

Results and Discussion

Deoxy Mb, MbCO, and Mb*CO. The $L_{2,3}$-edge experimental (upper curves) and simulated (lower curves) spectra for deoxy Mb, MbCO, and Mb*CO are shown in Figure 2. The $L_{2,3}$-edge spectrum for MbCO (Figure 2b) is relatively structureless, with an observed branching ratio of 0.59 ± 0.01. Conversely, the $L_{2,3}$-edge spectrum of deoxy Mb (Figure 2a) has a noticeable shoulder on the low-energy side of the L_3 maximum and a branching ratio of 0.69 ± 0.01, which is significantly higher than that for MbCO. For Mb*CO (Figure 2c), a branching ratio of 0.70 ± 0.01 is similar to deoxy Mb (0.69 ± 0.01), but the fine details in the L_3 spectrum reveal differences between deoxy Mb and Mb*CO. These differences are quantitated in Table 1.

The Fe^{II} in deoxymyoglobin (deoxy Mb) is known to be high spin ($S = 2$), while MbCO is a low-spin species ($S = 0$). This is well-known from theoretical studies,[52] as well as Mossbauer,[39,40] magnetic susceptibility,[53] and Raman[30−34] spectroscopies. However, the observed branching ratios for deoxy Mb (0.69) and MbCO (0.59) are both low in comparison with the respective theoretical values for Fe^{II} sites (0.78 for $S = 2$ and 0.67 for $S = 0$).[54,55] This difference is due in part to a higher average fluorescence yield in the L_2 versus the L_3 region. Recently, de Groot and co-workers observed a higher intensity ratio of L_2:L_3 for a Ni complex with fluorescence detection than with a total electron yield measurement.[22,56] Similar fluorescence distortion has also been proposed for all transition metal compounds.

One simple approach to this problem is to define a corrected branching ratio, as follow: $R_{cor} = (\alpha L_3)/(\alpha L_3 + L_2)$, where α is defined as the ratio of the average L_3 fluorescence yield to the average L_2 fluorescence yield for an Fe^{II} species. Assuming $\alpha = 1.4$, we obtain $R_{cor} = 0.76 \pm 0.01$ for deoxy Mb and $R_{cor} = 0.67 \pm 0.01$ for MbCO, both of which are close to the theoretical values for high-spin ($S = 2$) and low-spin ($S = 0$)

(48) Takano, T. *J. Mol. Biol.* **1977**, *110*, 569.
(49) Phillips, S. E. V. *J. Mol. Biol.* **1980**, *142*, 531.
(50) Kuriyan, J.; Wilz, S.; Karplus, M.; Petsko, G. A. *J. Mol. Biol.* **1986**, *192*, 133.
(51) Lever, A. B. P., *Inorganic Electronic Spectroscopy*; Elsevir: New York, 1984; p 26.
(52) Case, D. A.; Karplus, M. *J. Mol. Biol.* **1978**, *123*, 697.
(53) Roder, H.; Berendzen, J.; Bowne, S. F.; Frauenfelder, H.; Sauke, T. B.; Shyamsunder, E.; Weissman, J. B. *Proc. Natl. Acad. Sci. U.S.A.* **1984**, *81*, 2359.
(54) Moulin, C. C.; Rudolf, P.; Flank, A. M.; Chen, C. T. *J. Phys. Chem.* **1992**, *96*, 6196.
(55) van der Laan, G. *Phys. B* **1989**, *158*, 395.
(56) de Groot, F. M. F.; Arrio, M. A.; Sainctavit, P.; Cartier, C.; Chen, C. T. *Phys. B* **1995**, *209*, 84.

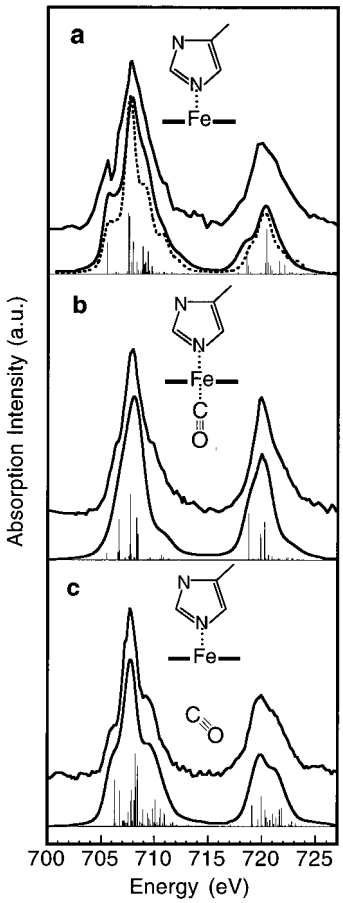

Figure 2. $L_{2,3}$-edge XAS spectra of (a) deoxy Mb, (b) MbCO, and (c) Mb*CO. For each figure, the upper curve is the experimental XAS spectrum while the lower curve is simulated using a ligand field multiplet calculation. The vertical lines are the multiplet transition intensities. The dashed line in part a represents the simulated spectrum where $D_t = 0$, for comparison with the best-fit simulation where $D_t = -0.1$ eV. The inserts represent the simplified local environment for the iron sites, with the bold line indicating the heme plane.

ferrous species, respectively. The same α applied to a previously reported high-spin Fe^{II} ($S = 2$) rubredoxin spectrum[24] yields a corrected branching ratio of 0.77, which is similar to the theoretical value for a high-spin, ferrous species. It seems approximately valid, therefore, that the yield ratio could be similar for other iron-containing molecules, i.e. other myoglobins. Based on this approach, Mb*CO has a R_{cor} of 0.77 ± 0.01 and is a high-spin species. The observed (R_{obs}) and corrected (R_{cor}) values for all of the myoglobin species studied here are listed in Table 1.

For simulating the L-edge spectra, we began with D_{4h} symmetry ($D_t = 0$). For MbCO, using this symmetry with $10D_q = 4.0$ and $D_s = 0.21$ leads to a simulated spectrum which is in close agreement with the experimental one. In contrast, for deoxy Mb, we were not able to reproduce the experimental spectrum, especially the strong, low-energy shoulder, by using $D_t = 0$ (Figure 2a, dashed curve). But, by using a weak field, with $10D_q = 1.0$ eV, $D_s = 0.25$ eV, and $D_t = -0.10$ eV, the simulated spectrum strongly resembles the experimental data. The fact that deoxy Mb does not fit a with $D_t = 0$ is in agreement with the significant displacement of the iron atom from the heme plane.[43] The dramatic change in $10D_q$ from deoxy Mb (1.0 eV) to MbCO (4.0 eV) is consistent with the high-spin to low-spin conversion when CO binds to deoxy Mb. The $10D_q$, D_s, and D_t parameters which lead to the best fits for the experimental spectra are summarized in Table 2. The 3d orbital energy gaps for deoxy Mb and MbCO, calculated using our $10D_q$ values, are within the error of the previous results by extended Hückel theory.[57]

Table 2. Parameters Used in Ligand Field Multiplet (LFM) Simulations Which Lead to the Best Fits to the Experimental XAS Spectra

	$10D_q$ (eV)	D_s (eV)	D_t (eV)
deoxy Mb	1.00	0.25	−0.10
MbCO	4.00	0.21	0
Mb*CO	1.00	0.20	0.03
MbO_2	3.50	0.22	−0.02
$Mb^* + O_2$	1.40	0.30	0.03
met Mb	1.00	0.15	0.02
MbN_3	2.75	0	0

Similar to deoxy Mb, the Mb*CO spectrum was simulated using a D_{4h} symmetry with $10D_q = 1.0$ eV, $D_s = 0.20$ eV, and $D_t = -0.03$ eV. In comparing the XAS spectra of deoxy Mb to Mb*CO, both similarities and differences are observed. The similar branching ratios and $10D_q$ values indicate a high-spin state for both species. However, the distortion parameters (D_s and D_t) for deoxy Mb are greater than for Mb*CO, indicating that deoxy Mb is more distorted from O_h symmetry than Mb*CO. This result is in agreement with crystallographic,[43] EXAFS,[11−13] and theoretical[58] data on Mb*CO at cryogenic temperature. These data all indicate that cryogenic temperatures prevent Mb*CO from relaxing to a full deoxy-like structure. This presumably reflects different degrees of distortion of the heme from planarity between the two states. As the sophistication of the calculations improves, a more direct correlation between electronic and molecular structure should be possible.

To illustrate how the distortion parameters determine the features of the calculated L-edge spectra, a series of calculations were performed for a high spin, ferrous species (like Mb*CO and deoxy Mb), varying one parameter (D_s or D_t) while fixing the remaining parameters (Figure 3). The dashed line represents the closest fit to the experimental data in each series. From these simulations, it is possible to roughly define the error for the distortion parameters as $D_s = 0.05$ eV and $D_t = 0.02$ eV. Therefore, the differences in parameters, especially D_t, between deoxy Mb and Mb*CO, appear to be significant. Finally, iron (3d) energy diagrams are constructed as shown in Figure 4 to further demonstrate the difference between Mb*CO and deoxy Mb.

MbCO and Mb*CO versus MbO_2 and Mb^*O_2. The experimental and theoretically simulated $L_{2,3}$-edge XAS spectra for MbO_2 and Mb^*O_2 are shown in Figure 5. Energy diagrams of the iron 3d orbitals for these two molecules are constructed as shown in Figure 6.

The XAS spectrum for MbO_2 (Figure 5a) is very similar to that of MbCO. The similar branching ratios (MbCO, 0.67 ± 0.01; MbO_2, 0.68 ± 0.01) and $10D_q$ values (MbCO, 4.0 eV; MbO_2, 3.5 eV) suggest low spin states ($S = 0$) for both species. The slightly smaller $10Dq$ value for MbO_2 is consistent with the weaker O_2 ligand and also consistent with the previous Hückel calculation which predicted a smaller 3d energy gap.[57] To date, there has been some question as to whether the spin state of MbO_2 is $S = 0$ or 1.[44,45,59,60] A spin state of $S = 1$ for MbO_2 would help explain the differences in reactivity between MbCO and MbO_2 because binding of oxygen to the deoxy Mb

(57) Eaton, W. A.; Hanson, L. K.; Stephens, P. J.; Sutherland, J. C.; Dunn, J. B. R. *J. Am. Chem. Soc.* **1977**, *100*, 4991.
(58) Srajer, V.; Reinisch, L.; Champion, P. M. *J. Am. Chem. Soc.* **1988**, *110*, 6656.
(59) Desbois, A.; Lutz, M.; Banerjee, R. *Biochemistry* **1979**, *18*, 1511.
(60) Frauenfelder, H.; Wolynes, P. G. *Science* **1985**, *229*, 337.
(61) Peisach, J.; Blumberg, W. E.; Ogawa, S.; Rachmilewitz, E. A.; Oltzik, R. *J. Biol. Chem.* **1971**, *246*, 3342.

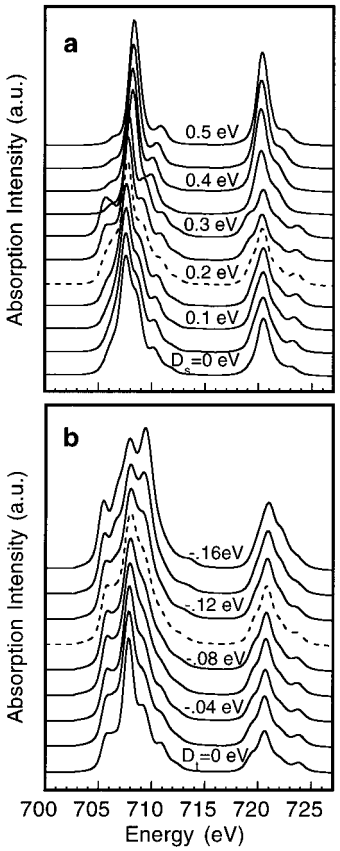

Figure 3. Demonstration of the sensitivity of the calculated $L_{2,3}$-edge spectra for a high-spin Fe^{II} species ($10D_q = 1.0$ eV) as one symmetry parameter (D_s or D_t) is varied while the other is fixed. In part a, $D_t = 0$ eV, while D_s is varied from 0.0 to 0.5 eV. In part b, $D_s = 0.25$ eV, while D_t is varied from 0.0 to -0.16 eV. The dashed lines represent the closest fits to the experimental data.

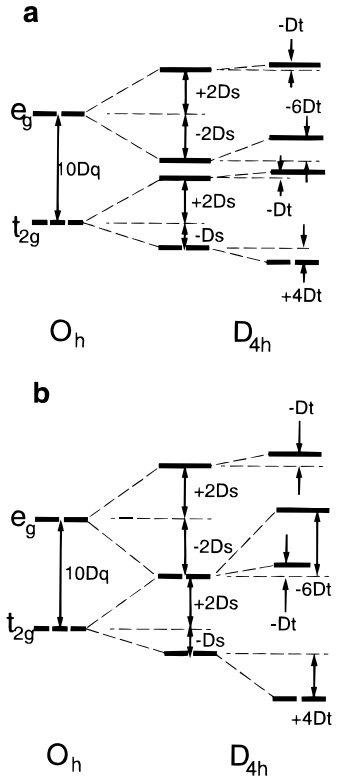

Figure 4. Proposed energy diagrams for the iron 3d orbitals for (a) Mb*CO and (b) deoxy Mb. The right-most column corresponds to a distorted D_{4h} symmetry.

species ($S = 2$) would involve a spin-state change of 1 for MbO_2, where it requires a spin-state change of 2 for MbCO. However, the data presented here do not support the earlier suggestions of an intermediate spin state for MbO_2 and indicate that, at least in the ground (ligand-bound) state, the spin states of MbCO and MbO_2 are the same (low spin).

Reactivity differences between MbCO and MbO_2 may also be due to unique intermediate (photoproduct) states. The observed $L_{2,3}$-edge XAS spectrum for MbO_2 before and after photolysis can be seen in Figure 5b. Chance and co-workers[28,44] have shown that the low-temperature quantum yield of photolysis for MbO_2 is 0.50 ± 0.05 at 8 K. Thus, in the spectrum, the observed photoproduct (Mb^*O_2) contains 50% ligand-bound material (MbO_2). The L-edge XAS spectrum for the photolyzed portion, designated $Mb^* + O_2$, was obtained by subtracting the ligand-bound fraction from the observed photoproduct spectrum: $Mb^* + O_2 = (Mb^*O_2 - 0.5MbO_2)$. The resulting difference spectrum can be seen in Figure 5c.

The extracted spectrum ($Mb^* + O_2$) has a main L_3 peak with side peaks on both the low and higher energy sides, a clear doublet L_2, and a branching ratio of 0.72 ± 0.02. Large differences between $Mb^* + O_2$ and low-spin MbO_2 are observed both in XAS spectra (Figure 5) and in the 3d energy diagram (Figure 6). Its branching ratio ($R_{cor} = 0.72 \pm 0.02$) and the $10D_q$ value (1.40 eV) are intermediate to the ligand-bound (MbO_2) and deoxy (Mb) states, suggesting an intermediate spin state for $Mb^* + O_2$. This intermediate spin is in contrast to Mb*CO, where the branching ratio and $10D_q$ value are deoxy-like, i.e. high spin. On the other hand, the distortion parameters, D_s and D_t, are greater for $Mb^* + O_2$ than for Mb*CO (Table 1). This result is in agreement with a more deoxy-like heme structure, which has also been observed in XANES spectra of $Mb^* + O_2$.[28] The electronic differences between Mb*CO and $Mb^* + O_2$ may help explain reactivity differences between the two species.

Fe(II) versus Fe(III) Species. EPR,[36−38] Mossbauer,[39] and X-ray K-edge studies[28] have indicated that when ligands bind to deoxy Mb, a significant transfer of electron density from the metal to the ligand occurs but do not indicate a formal $Fe^{III}L^-$ structure. The L_3- and L_2-edge positions of two ferric myoglobin species (met Mb and MbN_3), which are significantly higher than the ferrous species, also support this hypothesis (Figure 7). As with earlier K-edge data,[28] the L-edge positions shift to higher energy for the ferric species. This shift can be explained by an increased positive charge on the metal in the ferric myoglobins, which makes removal of a 2p electron more difficult, i.e. it requires higher excitation energy. Thus, L-edge measurements support the hypothesis that binding of CO or O_2 to deoxy Mb does not result in a full $Fe^{III}L^-$ species.

Examination of the $L_{2,3}$-edge spectra of met Mb and MbN_3 also provides a spin state comparison of ferric and ferrous myoglobins. MbN_3, which is low spin, has a prominent peak at the low-energy side of L_3 in its $L_{2,3}$-edge XAS spectrum and represents the transition of a 2p electron to the half-occupied t_{2g} (d_{xy}) orbital in the d^5 configuration. T_{2g} is filled in the ferrous, low-spin (d^6) configuration, and thus this transition is absent from low-spin, ferrous Mb spectra like MbCO. The branching ratio for MbN_3 ($R_{cor} = 0.67 \pm 0.01$) is the same as that for MbCO, which is consistent with a low-spin ($S = {}^1/_2$)[61] configuration. The branching ratio (0.76 ± 0.01) and $10D_q$ value (1.0 eV) for met Mb are the same as those for deoxy Mb, indicative of a high-spin, ferric species ($S = {}^5/_2$).[62]

Analysis of the complete series of high- and low-spin, ferric and ferrous state myoglobins demonstrates the power of L-edge

(62) Beetlestone, J.; George, P. *Biochemistry* **1954**, *3*, 707.

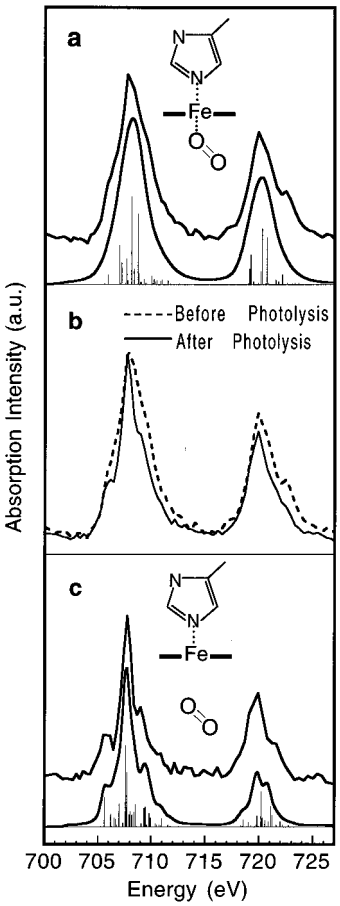

Figure 5. $L_{2,3}$-edge XAS spectra of (a) MbO_2, (b) MbO_2 (- - -) versus observed photoproduct Mb^*O_2 (—), and (c) the photolysis yield corrected $Mb^* + O_2$ (see text for details). For parts a and c, the upper curve is the experimental XAS spectrum while the lower curve is simulated using a ligand field multiplet calculation. The vertical lines are the multiplet transition intensities. For the simulated spectra, the vertical lines are the multiplet transition intensities. The inserts represent the simplified local environment for the iron sites, with the bold line indicating the heme plane.

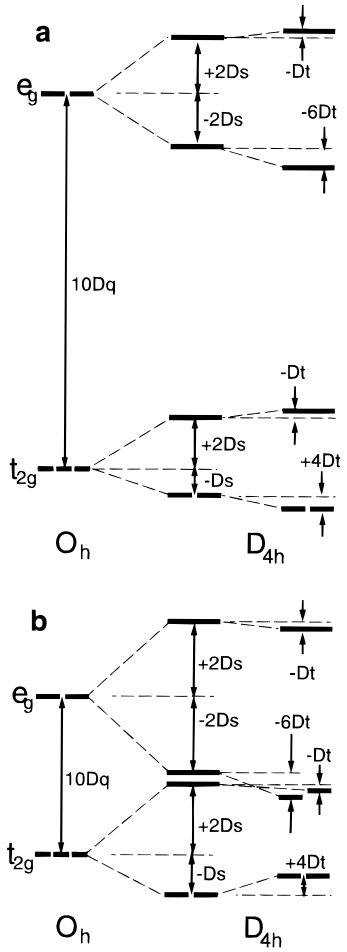

Figure 6. Proposed energy diagrams for the iron 3d orbitals for (a) MbO_2 and (b) $Mb^* + O_2$. The right-most column corresponds to a distorted D_{4h} symmetry.

XAS for addressing electronic differences in both the oxidation states and spin states of metalloproteins. Figure 8 summarizes the relationships between branching ratio and L_3-edge peak positions for low- and high-spin, ferrous and ferric iron proteins and model compounds. This diagram demonstrates how species with similar oxidation states and spin states, respectively, group together.

Advantages of L-Edge XAS As a Photolysis Probe. (a) L-Edge XAS versus Other Optical Probes. For the first-row transition metals, metal 3d orbitals are important in ligand-bonding. Therefore, a fundamental factor for determining many metalloprotein reaction mechanisms is an understanding of how the 3d orbital structure changes during the course of the metalloprotein reaction. For example, photon cleavage of chemical bonds between metal centers and their ligands alters the local symmetry and changes the electronic structure of metal 3d orbitals. Numerous spectroscopic methods use light to probe the 3d orbital structure in metalloproteins to provide complementary information. In hemeproteins, UV−visible absorption spectroscopy is able to detect d−d and metal−ligand charge transfer transitions, which can produce direct information on the iron.[27] However, these transitions often overlap with other transitions in the valence orbitals, such as porphyrin $\pi \rightarrow \pi^*$ transitions, and are hard to resolve. Infrared and Raman spectroscopies monitor the vibrational frequencies of the metal−ligand bonds, the diatomic ligand itself (CO, O_2, NO, etc.), and

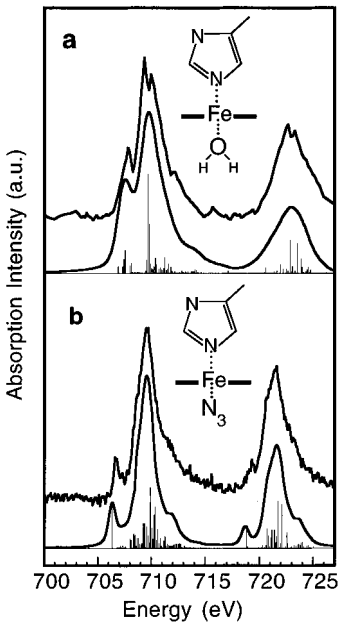

Figure 7. $L_{2,3}$-edge XAS spectra of the ferric (Fe^{III}) species: (a) met Mb and (b) MbN_3. For each part, the upper curve is the experimental XAS spectrum while the lower curve is simulated using a ligand field multiplet calculation. The vertical lines are the multiplet transition intensities. The inserts represent the simplified local environment for the iron sites, with the bold line indicating the heme plane.

the porphyrin ring.[29−32] These vibrational spectra provide information about metal−ligand bonding and bond strength, but

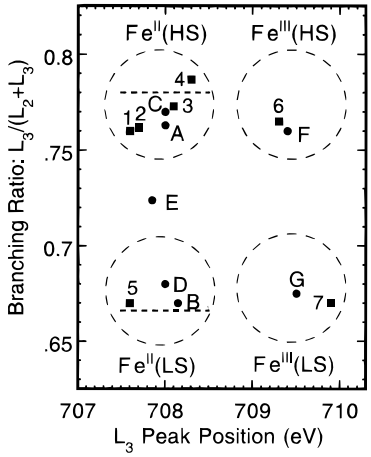

Figure 8. A summary diagram of the branching ratios and L_3-edge positions for various Fe^{II} and Fe^{III} proteins and model compounds. The solid circles represent the myoglobin species presented in this study, while the squares represent L-edge data from previously reported iron compounds. The dashed horizontal lines indicate the theoretical branching ratios for high-spin ($S = 2$) and low-spin ($S = 0$) Fe^{II} iron species. The dotted circles (with no defined radius) are guides to indicate regions of similar oxidation state and spin state. The detailed sample information is as follows: (A) deoxy Mb *(II, HS)*, (B) MbCO *(II, LS)*, (C) Mb*CO *(II, HS)*, (D) MbO_2 *(II, LS)*, (E) Mb* + O_2 (*II*, intermediate spin), (F) met Mb *(III, HS)*, (G) MbN_3 *(III, LS)*, (1) Fe*(II, HS)*(tppb), (2) Fe*(II, HS)* rubredoxin, (3) Fe*(II, HS)*(salpm), (4) Fe*(II, HS)*$(phen)_2(NCS)_2$ at 300 K, (5) Fe*(II, LS)*$(phen)_2(NCS)_2$ at 77 K, (6) Fe*(III, HS)* rubredoxin, and (7) [Fe*(III, LS)*$(HB(pz)_3)_2$][ClO_4].

only indirectly address the 3d orbital structure of the metal center. Electron paramagnetic resonance (EPR) spectroscopy[36−38] is metal specific; however, this technique relies on a paramagnetic (high spin) metal center; diamagnetic systems are EPR silent. In comparison, L-edge XAS monitors the transition from a core metal orbital (2p) to an unoccupied orbital (3d), which makes it sensitive to all metal centers with an unoccupied 3d orbital, and is a direct probe of the 3d orbital occupancy of that metal center.

(b) L-Edge versus K-Edge Probe. For 3d transition metals, L-edge XAS is a more sensitive probe of electronic structures involving metal (3d) orbitals,[19] while K-edge XAS is more sensitive to the molecular structure surrounding the metal, *e.g.*, coordination information. For monitoring photochemically sensitive metal 3d orbitals, L-edge XAS is advantageous over K-edge XAS. L-edge spectra possess rich multiplets due to the interactions between the 2p core hole and the 3d electrons—which are smaller in K-edge spectra. The highly-structured multiplets provide a full range of electronic information, including metal 3d orbital splitting, oxidation states, and spin states, all of which are important for a photochemical process. Also, the 2p → 3d transition is dipole-allowed, making the transition intense and more sensitive to the photochemical events that often alter metal (3d) orbitals. In comparison, the 1s → 3d transition is dipole-forbidden and weak, and only occurs under certain circumstances, such as a quadrupole transition or by p−d orbital mixing. A comparison of these two transitions[63−65] (2p → 3d versus 1s → 3d) for Mb*CO can be clearly seen in Figure 9. Finally, the line widths for soft X-ray transitions are usually 3−5 times better than at hard X-ray edges, which results in a sharper XAS spectrum.

(63) K-edge XANES spectrum of Mb*CO was recorded in a separate experiment in this laboratory using a kilohertz laser (Photonics Industries, GM-30).

(64) Wang, H.; Peng, G.; Cramer, S. P. Manuscript in preparation.

(65) Bergsma, S. C.; Li, X.; Kassner, M. E. *J. Mater. Eng. Perform.* **1996**, *5*, 100.

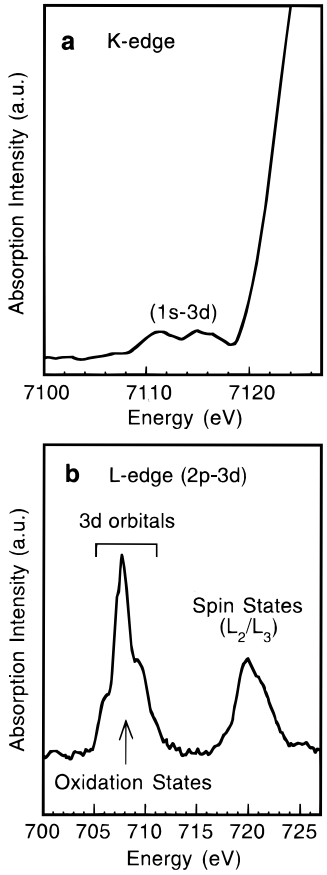

Figure 9. (a) The pre-K-edge (1s → 3d) and (b) L-edge (2p → 3d) XAS spectra for Mb*CO. A more detailed and sharper multiplet feature is demonstrated in the L-edge XAS.

(c) Calculable Multiplet. For relatively ionic complexes, 3d transition metal L-edge XAS multiplets, which are due to the 2p core hole and 3d electron interaction, can be well-characterized with an atomic orbital approximation and ligand field multiplet theory. For more covalent species, procedures allowing for configuration interaction are available.[21] Thus, these calculations can provide information about 3d orbital structure, which is essential for understanding the reaction mechanisms of many photochemical and photobiological processes. This is especially true in the case of ligand-binding and release, where the metal 3d orbitals are involved in bonding, and elucidating 3d orbital structure provides a fundamental understanding of the ligand-binding process.

Our $L_{2,3}$-edge spectra for myoglobin demonstrate the value of calculable XAS multiplets. (1) The differences in the L-edge XAS of Mb*CO and deoxy Mb look minor, but the ligand field calculation indicates significant differences in the Fe (3d) electronic structure for the two species, suggesting that Mb*CO is an intermediate state that is different from deoxy Mb. (2) The XAS simulations also demonstrate that Mb*CO and Mb* + O_2 are quite different intermediate states, which lead to unique ligand-rebinding mechanisms. (3) The simulations also distinguish between high-spin and low-spin, Fe^{II} and Fe^{III} species, and thus provide a method for observing oxidation state and spin state changes during photochemical reactions. In short, a calculable XAS multiplet is crucial for interpreting experimental L-edge XAS spectra in a more detailed and thorough manner.

Conclusions

Using MbCO and MbO_2, we report the first experiment that utilizes first-row transition metal L-edge XAS for probing

biological photolysis products. Our analysis indicates that MbCO and MbO_2 are both low spin, which does not support some previous results of an intermediate spin for MbO_2. At cryogenic temperatures, Mb*CO has the same spin state (high spin) as deoxy Mb but does not relax to a complete deoxy-like configuration. In addition, Mb*CO is different from Mb* + O_2, the latter of which appears to have a spin state intermediate to that of deoxy Mb and MbO_2. The difference in 3d orbital configuration, which results in this different spin state for Mb*CO and Mb* + O_2, may help explain the differences in reactivity between the two species. The oxidation states of ligand-bound and photolyzed myoglobins have also been addressed.

Soft X-ray (L-edge) absorption spectroscopy has many advantages over hard X-ray (K-edge) spectroscopy and other optical probes for the characterization of photoproduct intermediate states. These advantages include (1) a direct and metal-selective probe for all metalloproteins, (2) intense, dipole-allowed transitions ($2p \rightarrow 3d$) to the ligand-bonding orbitals, (3) higher X-ray energy resolution that provides more structural details, and (4) a calculable XAS multiplet for a detailed analysis of d-orbital configurations. A calculable XAS multiplet is especially important for understanding L-edge data from a fundamental point of orbital theory. Overall, our experiments demonstrate the strength of L-edge XAS for studying metalloprotein photolysis intermediates at a fundamental level.

Acknowledgment. This work was supported by the Lawrence Berkeley National Laboratory, Laboratory Directed R&D Fund; by the Department of Energy, Office of Health and Environmental Research; and by The National Institutes of Health (GM-44380 to S.P.C. and HL-45892 to M.R.C). L.M.M. is supported by a University of California President's Postdoctoral Fellowship. The Stanford Synchrotron Radiation Laboratory is funded by the Department of Energy, Office of Basic Energy Science.

JA961446B